The FEBS Journal

FEBS PRESS science publishing by scientists

Comparison of human glutamate carboxypeptidases II and III reveals their divergent substrate specificities

Michal Navrátil[1,2], Jan Tykvart[1,2], Jiří Schimer[1,2], Petr Pachl[1], Václav Navrátil[1,2], Tibor András Rokob[3], Klára Hlouchová[1,2], Lubomír Rulíšek[1] and Jan Konvalinka[1,2]

1 Institute of Organic Chemistry and Biochemistry, Gilead Sciences and IOCB Research Centre, Academy of Sciences of the Czech Republic, Prague, Czech Republic

2 Department of Biochemistry, Faculty of Natural Sciences, Charles University in Prague, Czech Republic

3 Institute of Organic Chemistry, Research Centre for Natural Sciences, Hungarian Academy of Sciences, Budapest, Hungary

Keywords

arene-binding site; GCPIII; prostate-specific membrane antigen; QM/MM calculations; β-citryl-L-glutamate

Correspondence

J. Konvalinka, Institute of Organic Chemistry and Biochemistry, Gilead Sciences and IOCB Research Centre, Academy of Sciences of the Czech Republic, Flemingovo n. 2, 166 10 Prague, Czech Republic

Fax: +420 220 183 578

Tel: +420 220 183 218

E-mail: konval@uochb.cas.cz

(Received 10 March 2016, revised 25 April 2016, accepted 18 May 2016)

doi:10.1111/febs.13761

Glutamate carboxypeptidase III (GCPIII) is best known as a homologue of glutamate carboxypeptidase II [GCPII; also known as prostate-specific membrane antigen (PSMA)], a protease involved in neurological disorders and overexpressed in a number of solid cancers. However, mouse GCPIII was recently shown to cleave β-citrylglutamate (BCG), suggesting that these two closely related enzymes have distinct functions. To develop a tool to dissect, evaluate and quantify the activities of human GCPII and GCPIII, we analysed the catalytic efficiencies of these enzymes towards three physiological substrates. We observed a high efficiency of BCG cleavage by GCPIII but not GCPII. We also identified a strong modulation of GCPIII enzymatic activity by divalent cations, while we did not observe this effect for GCPII. Additionally, we used X-ray crystallography and computational modelling (quantum and molecular mechanical calculations) to describe the mechanism of BCG binding to the active sites of GCPII and GCPIII, respectively. Finally, we took advantage of the substantial differences in the enzymatic efficiencies of GCPII and GCPIII towards their substrates, using enzymatic assays for specific detection of these proteins in human tissues. Our findings suggest that GCPIII may not act merely as a complementary enzyme to GCPII, and it more likely possesses a specific physiological function related to BCG metabolism in the human body.

Database

The X-ray structure of GCPII Glu424Ala in complex with BCG has been deposited in the RCSB Protein Data Bank under accession code 5F09.

Abbreviations

3D, three-dimensional; AAS, atomic absorption spectroscopy; ABS, arene-binding site; ACN, acetonitrile; BCG, β-citryl-L-glutamic acid (β-citrylglutamate, beta-citrylglutamate, beta-citryl-L-glutamic acid, beta-citryl-L-glutamate); BSA, bovine serum albumin; C12E8, octaethylene glycol monododecyl ether; DBU, 1,8-Diazabicycloundec-7-ene; DIEA, N,N-Diisopropylethylamine; EtOAc, ethylacetate; $FolGlu_n$, folyl-*n*-γ-L-glutamic acid; G3PDH, glyceraldehyde 3-phosphate dehydrogenase; GCPII, glutamate carboxypeptidase II; GCPIII, glutamate carboxypeptidase III; HPLC, high-performance liquid chromatography; HRMS, high-resolution mass spectrometry; MeOH, methanol; MD/MM, molecular dynamical/molecular mechanical calculations; NAAG, *N*-acetyl-L-aspartyl-L-glutamic acid; NMR, nuclear magnetic resonance; OPA, orthophtalaldehyde; ORF, open reading frame; Pd(C), palladium on activated charcoal; PSMA, prostate-specific membrane antigen; QM/MM, quantum mechanical and molecular mechanical calculations; QM/MM/MD, quantum mechanical, molecular mechanical and molecular dynamical calculations; qPCR, quantitative polymerase chain reaction; rhGCPII, recombinant human glutamate carboxypeptidase II; SDS/PAGE, sodium dodecylsulfate polyacrylamide gel electrophoresis; TFA, trifluoroacetic acid; TLC, thin-layer chromatography.

Introduction

Glutamate carboxypeptidase III (GCPIII) is a binuclear zinc metallopeptidase that belongs to the MEROPS M28B peptidase subfamily (ID M28.012) [1]. GCPIII shares 67% sequence identity and 81% sequence similarity with glutamate carboxypeptidase II (GCPII, EC 3.4.17.21), one of the most well-characterized members of the M28B subfamily [2]. Additionally, GCPIII adopts an almost identical 3D structure and possesses very similar enzymatic activity to GCPII [3]. It is also predicted to be a type II transmembrane protein with amino acids 9–31 forming the transmembrane part of the structure [4] and its protease domain facing the extracellular milieu.

The physiological functions of GCPII include degradation of *N*-acetyl-L-aspartyl-L-glutamate (NAAG, Fig. 1), the most abundant peptide neurotransmitter in the brain [3,5], and processing of polyglutamylated folates ($FolGlu_n$, Fig. 1), vitamin B9 precursors, enabling the absorption of free folate in the small intestine [6,7]. Furthermore, GCPII, also known as prostate-specific membrane antigen (PSMA), has been investigated as a promising prostate cancer marker [8,9] and an interesting molecular address for specific anticancer drug delivery [10,11]. Because both GCPII and GCPIII have similar enzymatic activities and there is no specific monoclonal antibody against GCPIII [12], unravelling the distinct physiological functions of GCPII and GCPIII has been challenging.

Until recently, GCPIII was recognized mainly as a potentially complementary enzyme to GCPII. However, in 2011, Collard *et al.* [13] identified a novel physiological substrate for mouse GCPIII, β-citryl-L-glutamic acid (BCG, Fig. 1), which is cleaved to citrate and L-glutamate by GCPIII but not GCPII. Interestingly, the study also showed that the efficiency of NAAG vs. BCG cleavage by GCPIII is metal-dependent. The presence of zinc or manganese ions facilitates NAAG cleavage, and the presence of calcium or manganese ions facilitates cleavage of BCG. The researchers hypothesized that the ability of GCPIII to cleave BCG in the presence of specific metal ions may be caused by replacement of one of its two active site zinc ions by these metals [13].

BCG was first identified as a physiologically relevant molecule in the 1970s, when it was isolated from newborn rat brains [14]. Additionally, BCG-hydrolysing activity, as well as BCG itself, has been detected in rat testes [15,16]. Although BCG has been known for several decades, its precise physiological function remains unclear. One hypothesis suggested that BCG may serve as an endogenous low-molecular-weight chelator of iron or other biogenic metals [17]. However, the recent unambiguous assignment of BCG-hydrolysing activity to GCPIII increased the potential for elucidation of BCG's physiological role. Furthermore, the identification of GCPIII as a BCG hydrolase suggests that GCPIII may not function merely as a compensatory enzyme for GCPII, but may play a different, physiologically relevant role in humans.

We have shown previously that the GCPII tissue expression profile differs in human and animal models, which might have implications for its specific roles [18]. The findings concerning GCPIII/BCG metabolism have been obtained using animal models, mostly mice or rats. GCPIII tissue distribution in the human body is unknown, and it is crucial to validate and properly characterize this novel metal-dependent enzymatic activity for human GCPIII. Therefore, we set out to perform a careful comparative analysis of human GCPII and GCPIII activities towards their physiological substrates NAAG, BCG and polyglutamylated folates. Additionally, we describe the binding of BCG into the active sites of GCPII and GCPIII using X-ray crystallography and high-level (QM/MM) molecular modelling, respectively. Finally, employing the enzymological data, we were able to specifically detect GCPII and GCPIII protein levels in human tissues, a feat that had been impossible to achieve so far.

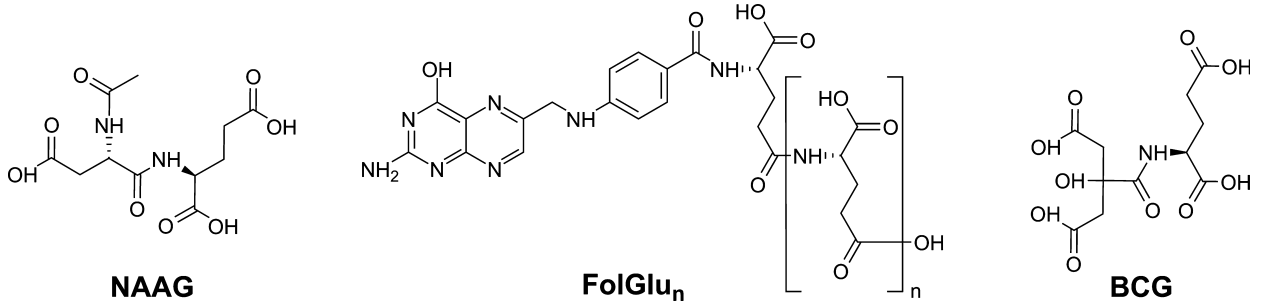

Fig. 1. Chemical structures of investigated substrates. From left to right: *N*-acetyl-L-aspartyl-L-glutamic acid (NAAG), *n*-γ-L-glutamylated folic acid ($FolGlu_n$) and β-citryl-L-glutamic acid (BCG).

Specific molecular recognition of these two close enzyme homologues will enable the use of GCPII as a selective molecular address for the anticancer drug delivery and to validate its potential for the diagnosis and prognosis of prostate cancer.

Results

BCG hydrolysis by GCPIII depends on divalent metal cations

Using recombinant human GCPII and GCPIII [19], we analysed hydrolysis of three physiological substrates in the presence or absence of calcium, manganese(II) and zinc cations. The chemical structures of the tested compounds, NAAG, $FolGlu_n$ and BCG are shown in Fig. 1.

The enzymological data, summarized in Fig. 2, indicate that BCG is selectively hydrolysed by human GCPIII. Although it is also cleaved by GCPII, the catalytic efficiency for the GCPIII-catalysed reaction is up to five orders of magnitude greater [Fig. 2A, k_{cat}/K_M (GCPII) = 1.7×10^2 $s^{-1}\cdot M^{-1}$ vs. k_{cat}/K_M (GCPIII, Ca^{2+}) = 1.33×10^7 $s^{-1}\cdot M^{-1}$]. Additionally, we found that the catalytic efficiency of human GCPIII is highly metal-dependent. The presence of calcium ions increased the BCG cleavage efficiency by two orders of magnitude [k_{cat}/K_M (GCPIII) = 1.8×10^5 $s^{-1}\cdot M^{-1}$ vs. k_{cat}/K_M (GCPIII, Ca^{2+}) = 1.33×10^7 $s^{-1}\cdot M^{-1}$], while zinc ions facilitated NAAG and $FolGlu_1$ cleavage [k_{cat}/K_M (GCPIII, NAAG) = 2.16×10^5 $s^{-1}\cdot M^{-1}$ vs. k_{cat}/K_M (GCPIII, NAAG, Zn^{2+}) = 2.27×10^6 $s^{-1}\cdot M^{-1}$]. Manganese ions seemed to increase GCPIII activity towards all tested substrates. The activation effect of these divalent cations is mainly driven by an increase in k_{cat} values, while the K_M values are less affected (Fig. 2B,C). Importantly, we also tested the ability of these cations to activate GCPII, and we did not observe any notable metal-dependent activity (data not shown).

These data suggest that in the presence of calcium cations, GCPII and GCPIII can be specifically detected based on their different enzymatic activities.

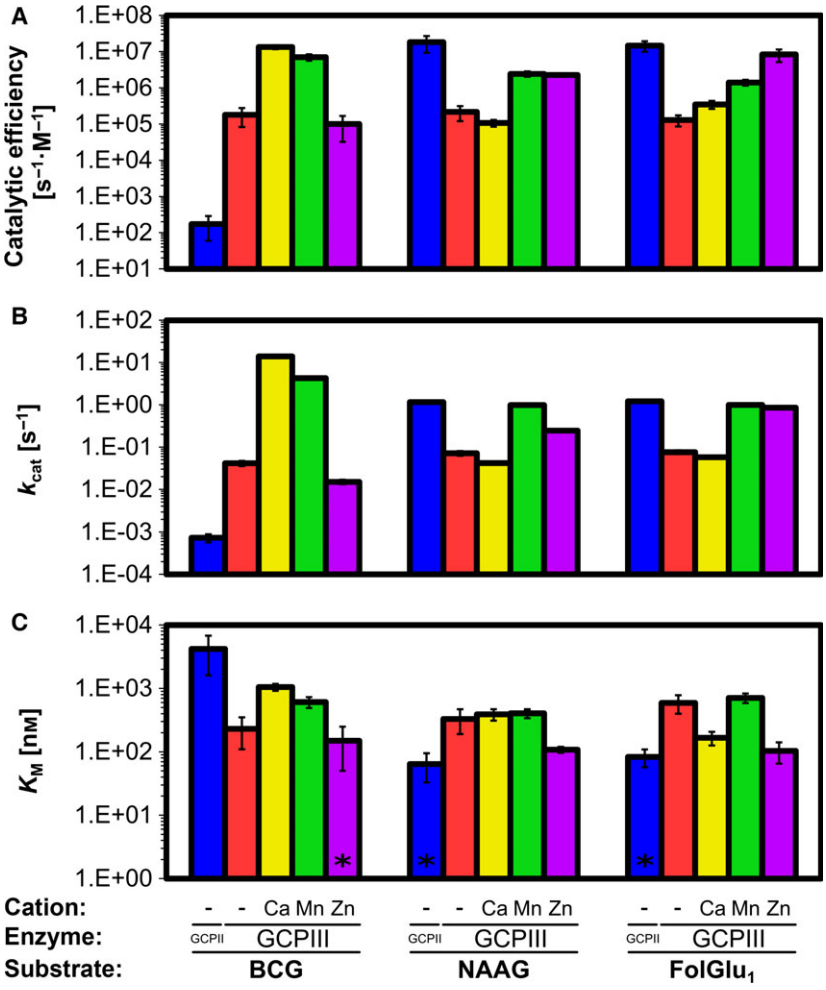

Fig. 2. Characterization of BCG-, NAAG- and $FolGlu_1$-hydrolysing activity of GCPIII in the absence or presence of divalent cations (Ca^{2+}, Mn^{2+} or Zn^{2+}) and comparison to GCPII. The reaction buffer was 25 mM bistrispropane, pH 7.5, supplemented with the cations where specified (Ca^{2+} 2.5 mM, Mn^{2+} 0.25 mM and Zn^{2+} 0.10 mM). Error bars represent SD. K_M and k_{cat} values were obtained by nonweighted hyperbolic fit into a single saturation curve consisting of 6–11 data points (n = 1). The panels show comparisons of (A) catalytic efficiencies, (B) k_{cat} values and (C) K_M values of GCPIII and GCPII towards the panel of substrates BCG, NAAG and $FolGlu_1$ in the presence or absence of calcium, manganese and zinc ions. Asterisks indicate that the K_M value was lower than the lowest substrate concentration (see Materials and methods for more information).

GCPII processes NAAG or $FolGlu_1$ with a two order of magnitude higher catalytic efficiency than GCPIII, while GCPIII processes BCG with a five order of magnitude higher catalytic efficiency than GCPII.

The GCPII arene-binding site facilitates processing of polyglutamylated folates

The GCPII structure includes an exosite called the arene-binding site (ABS), which comprises Arg463, Arg511 and Trp541 and is involved in the binding of the pteroate moiety during the cleavage of glutamylated folates [7,20]. A similar feature has not been described in the structure of GCPIII. We investigated the catalytic efficiency of GCPIII towards polyglutamylated folates ($FolGlu_{1–6}$), which bind to the ABS of GCPII, and compared it with previous data on GCPII cleavage efficiency of $FolGlu_{1–6}$ [7]. As shown in Fig. 3, GCPIII processes $FolGlu_{2–6}$ with much lower catalytic efficiency than GCPII, while processing of monoglutamylated folate ($FolGlu_1$) is comparable between the two enzymes (Fig. 3A). The difference resides mainly in the higher K_M values for GCPIII (Fig. 3B,C). These results are in good agreement with previously reported structural data showing that GCPII is unable to fully utilize the ABS for binding of the pteroate moiety of $FolGlu_1$, while the $FolGlu_{2–3}$ substrates are able to bind into this exosite [7].

Occupancy of active site zinc ions is lower for GCPIII than GCPII

The previously reported X-ray structures of GCPIII suggested that the active site Zn1 and Zn2 atoms have only partial occupancies in the 0.80–0.95 and 0.45–0.80 ranges, respectively [21]. To further corroborate these findings, we applied an atomic absorption spectroscopy technique to GCPII and GCPIII to determine the precise amount of zinc atoms per molecule (for experimental details, see Materials and methods). We determined that GCPII contains 1.40 zinc atoms per molecule and GCPIII contains 1.13. These results further support the partial occupancy of Zn2 within the GCPIII structure.

BCG binding mode in the GCPII active site: X-ray structure

To elucidate the differences in BCG cleavage by GCPII and GCPIII, we prepared a diffraction-quality crystal of inactive GCPII Glu424Ala in complex with BCG. We solved the structure by molecular replacement and refined the final model to 1.85 Å resolution

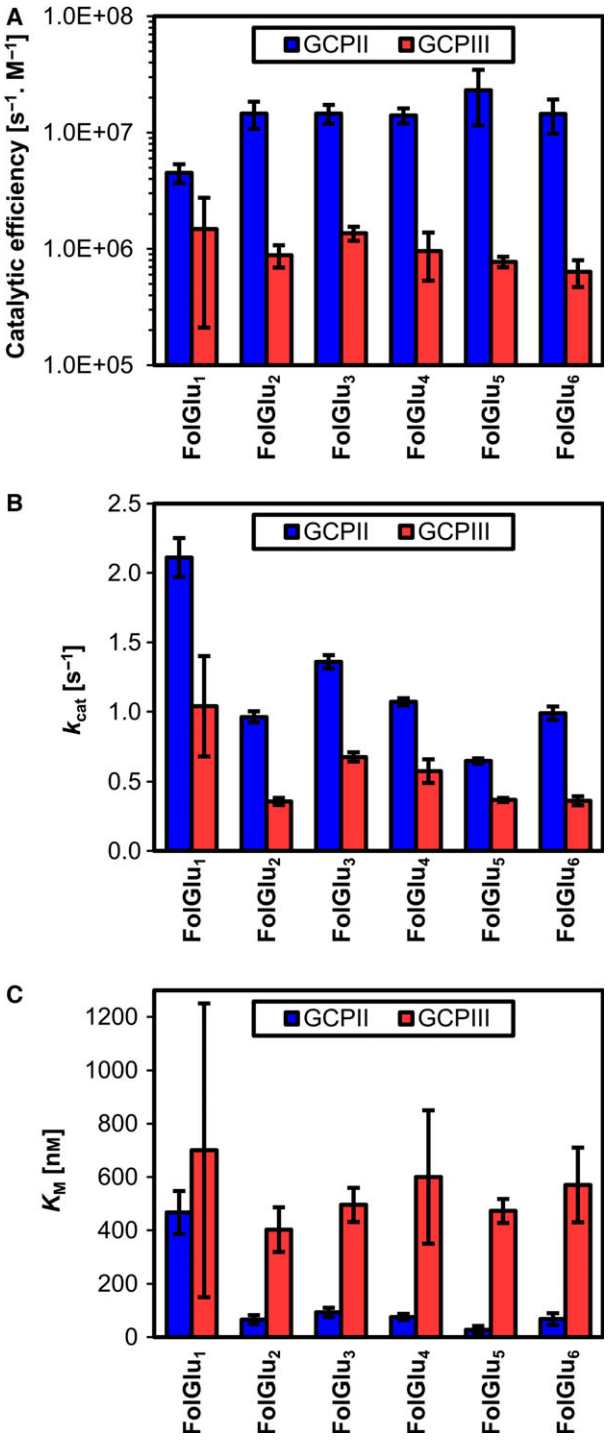

Fig. 3. Comparison of the $FolGlu_{1–6}$-hydrolysing activity of GCPIII and GCPII: (A) catalytic efficiencies, (B) k_{cat} values and (C) K_M values. The reaction buffer was 25 mM Tris/HCl, pH 7.5, without any added cations. Data for cleavage of $FolGlu_{1–6}$ by GCPII were measured previously [7]. Error bars represent SD. K_M and k_{cat} values were obtained by nonweighted hyperbolic fit into a single saturation curve consisting of 6–10 data points (n = 1).

Table 1. Data collection and refinement statistics.

Compound	BCG
PDB ID	5F09
Data collection statistics	
Space group	*I222*
Cell parameters	
a (Å)	100.899
b (Å)	130.916
c (Å)	159.118
α, β, γ (°)	90,90,90
No. of molecules in AU	1
Wavelength (Å)	0.918
Resolution (Å)	1.85
Highest resolution shell (Å)	1.96–1.85
No. of unique refl.	89 051 (13 967)
Multiplicity	4.51 (4.43)
Completeness (%)	98.8 (97.1)
R_{meas} (%)[a]	8.1 (94.1)
Average I/σ (I)	13.29 (1.96)
Wilson B (Å^2)[b]	39.43
Refinement statistics	
Resolution range (Å)	30.00–1.85
Highest resolution shell (Å)	1.90–1.85
No. of refl. in working set	84 147 (4444)
No. of refl. in test set	6105 (322)
R value (%)[c]	0.155 (0.311)
R_{free} value (%)[d]	0.181 (0.336)
RMSD bond length (Å)	0.014
RMSD angle (°)	1.690
No. of atoms in AU	6402
No. of protein atoms in AU	5804
No. of ligand atoms in AU	22
No. of ion atoms in AU	4
No. of water molecules in AU	562
Mean B value (Å^2)	21.91
Ramachandran plot statistics[e]	
Res. in favoured regions (%)	97.2
Res. in allowed regions (%)	2.7
Outliers	Val382

The data in parentheses denote the highest resolution shell. [a]R_{meas} is the redundancy-independent merging R factor [25]. [b]Estimated by SFcheck [26,27]. [c]R value = $||F_o| - |F_c||/|F_o|$, where F_o and F_c are the observed and calculated structure factors, respectively. [d]R_{free} is equivalent to R value but is calculated for 5% of the reflections chosen at random and omitted from the refinement process. [e]As calculated by MolProbity [28,29]. The AviTEV-tag and first 11 amino acids from the extracellular part of GCPII are not visible in the structure.

(PDB ID 5F09; data collection and refinement statistics are shown in Table 1). The binding mode of BCG within GCPII is depicted in Fig. 4A. The glutamate moiety of BCG binds into the S1′ pocket of GCPII in an identical manner as described for FolGlu$_n$ or NAAG substrates [7,22]. It forms hydrogen bonds with the side chains of Arg210, Asn257 and Tyr552, and also with Lys699 and Tyr700 forming the so-called 'glutarate sensor' [23]. However, in this structure, the glutamate moiety shows weaker electron density (see Fig. 4B) than in crystal structures of complexes with better substrates (e.g. FolGlu$_n$ or NAAG [7,22]). Interestingly, the glutarate sensor adopts two equally populated conformations, the 'closed' and 'open' form (see Fig. 4C). Unlike the glutamate moiety, the citrate moiety of BCG forms only one identifiable interaction with the enzyme: a salt bridge between one of the citrate carboxyl groups and the guanidine group of Arg534. This lack of interaction in the S1 pocket may be responsible for the substantially lower affinity of BCG towards GCPII, compared to that of other substrates such as NAAG. Accordingly, the citrate moiety of BCG had much less well-defined electron density than the glutamate moiety (see Fig. 4B), suggesting that this portion of BCG is not present in one particular conformation within the GCPII active site and likely possesses some degree of rotational freedom. These findings suggest that the binding of BCG, and in particular its citrate moiety, into the GCPII active site might partially prevent the closing of the glutarate sensor. Finally, it should be noted that we refined BCG to 70% occupancy, which is yet another indication that the binding affinity of BCG for GCPII is poor.

BCG binding mode in the GCPIII active site: QM/MM calculations

The technical difficulties of obtaining diffraction-quality crystals for GCPIII in complex with BCG led us to approximate the structure of GCPIII in complex with BCG by quantum mechanics/molecular mechanics (QM/MM). We computed a QM/MM homology model of GCPIII in complex with BCG (see Fig. 5A). The comparison of the obtained GCPII and GCPIII structures in complex with BCG suggests that the overall binding mode of this substrate is very similar in both enzymes (see Fig. 5B). However, in contrast to the flexibility of the BCG citrate moiety in the structure of the GCPII-BCG complex, both citrate carboxylates are coordinated – specifically by Ser444, Arg524 and Arg526 in the QM/MM model of GCPIII. Additionally, the orientation of the BCG hydroxyl group in GCPIII enables its coordination by Gly508. In the GCPII-BCG structure, the orientation of this hydroxyl group is different, and prevents such an interaction.

Thermodymamics of Zn^{2+}/Ca^{2+} binding in the active site: QM/MM calculations

After obtaining plausible QM/MM models of GCPIII in complex with NAAG and BCG, it is

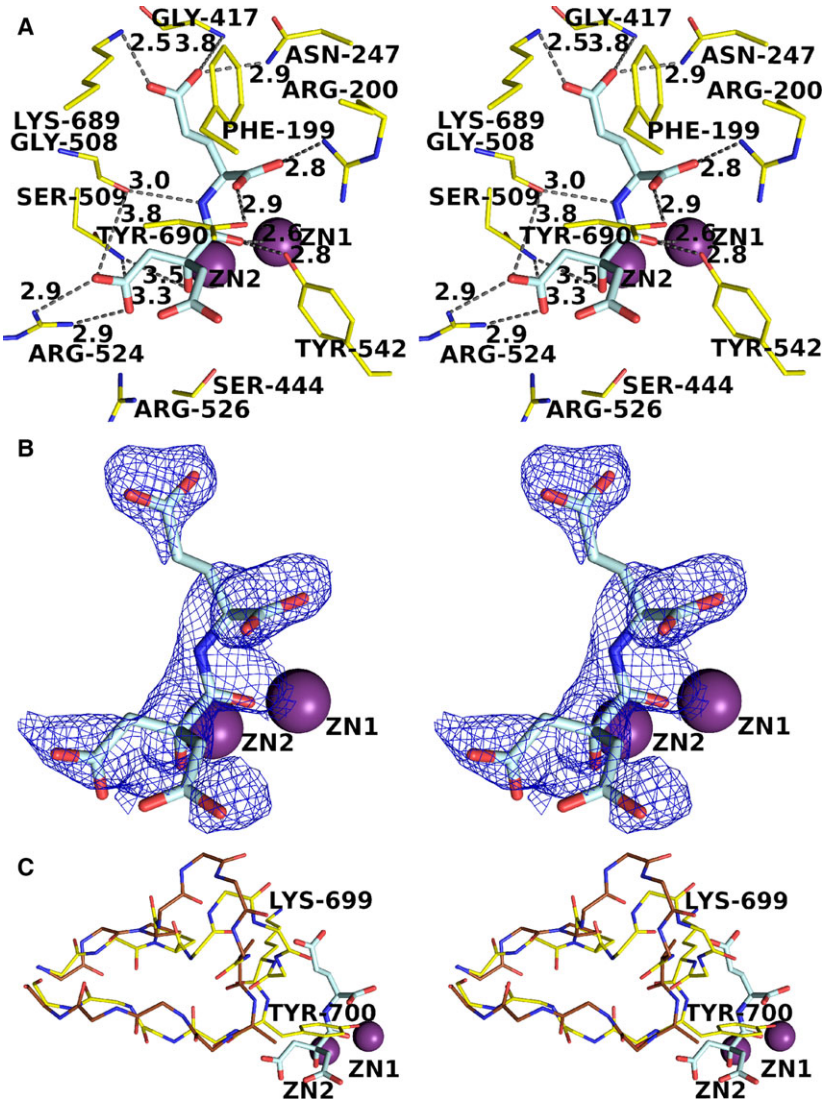

Fig. 4. X-ray structure of GCPII Glu424Ala in complex with β-citryl-L-glutamic acid (BCG, PDB ID 5F09). Images are rendered in cross-eye stereo representation. Active site zinc ions are shown in violet, GCPII protein in yellow and BCG in pale cyan. In panel (A), Tyr700 is truncated to provide an unobscured view. Distances are shown in Å. Images were created using PYMOL [24]. (A) Detail of the active site of GCPII with bound BCG. (B) The electron density map $2F_o - F_c$ for BCG in the GCPII-BCG complex (PDB ID 5F09), contoured at 1.0σ. (C) The structure of GCPII in complex with BCG features the glutarate sensor in two conformations, closed (yellow) and open (brown). Glutarate sensor is depicted as main chain only except for Lys699 and Tyr700 (only stubs are shown for the open conformation).

computationally straightforward to address the possibility of replacing one Zn^{2+} in the active site with a Ca^{2+} ion. This hypothesis has been put forward previously [13], and here, we tested it using advanced QM/MM modelling, which is arguably more rigorous and accurate than MD/MM simulations (or even less elaborate models [13]). We surmised that the QM/MM equilibrium structures and associated energetics may provide structural definition of potential calcium binding in the GCPII/III active site as well as a clue to explaining the observed differences in catalytic efficiency of GCPII and GCPIII in the absence or presence of Ca^{2+}. We carried out 12 QM/MM simulations varying the enzyme (GCPII and GCPIII), substrate (NAAG and BCG) and active site metals (Zn1–Zn2, Ca1–Zn2, Zn1–Ca2). Eight of the QM/MM equilibrium geometries (optimized structures, Zn1–Zn2, Zn1–Ca2) for the QM part (~ 280 atoms comprising the active site) are deposited in Data S1. In brief, substitution of Ca^{2+} for Zn^{2+} in the Zn2 position (which is in all cases favoured by approximately 10–15 kcal·mol^{-1} compared to Ca1-Zn2 structures) induces several structural perturbations to the active site (see Fig. 6). In comparison with the X-ray structure of GCPII in complex with BCG (PDB ID 5F09), the heterometallic cluster Zn1-Ca2 is rotated relative to the homometallic Zn1-Zn2 cluster so that Ca2 can be bound in a typical pentagonal bipyramidal manner, whereby His367 and a partially ionized hydroxyl of the citrate moiety are the axial ligands. An active site water forms part of the pentagonal coordination base, and residues Asp443 and Asp377 are correspondingly shifted to accommodate the Ca2 atom. Finally, we compared the energetics of calcium binding in the

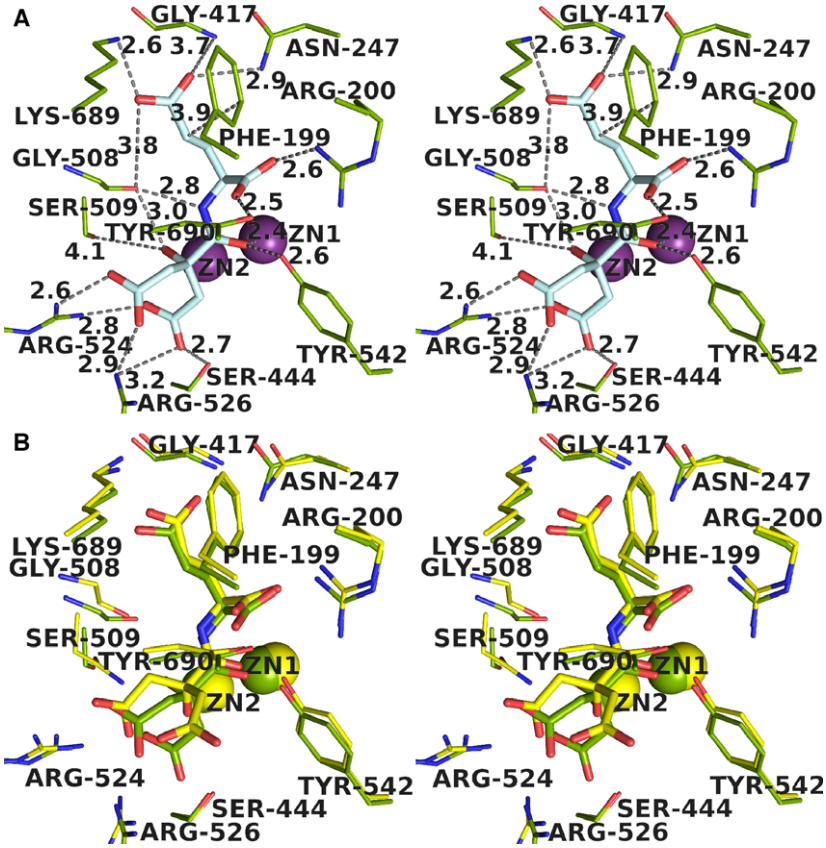

Fig. 5. QM/MM model of GCPIII in complex with BCG and its comparison to the X-ray structure of GCPII Glu424Ala in complex with β-citryl-L-glutamic acid (BCG, PDB ID 5F09). Images are rendered in cross-eye stereo representation. Numbering of amino acid residues in GCPIII is lower by 10 in comparison to GCPII. Tyr700/Tyr690 is truncated to provide an unobscured view. Distances are shown in Å. Zinc atoms are shown as spheres. Images were created using PYMOL [24]. (A) The QM/MM model of GCPIII in complex with BCG shows that GCPIII binds BCG in a way that allows more interactions. Protein is coloured green, BCG pale cyan, zinc atoms violet. (B) Overlay of GCPII-BCG complex with the QM/MM model of GCPIII-BCG complex. It shows that BCG is bound in a very similar manner to both GCPII and GCPIII. The only two differences are the presence of Ser509 in GCPIII instead of Asn519 in GCPII and how the citrate moiety is bound. GCPII-BCG complex is coloured yellow, and GCPIII-BCG in green.

GCPII and GCPIII sites in the presence of substrate (BCG vs. NAAG). Employing the QM (DFT+D3/TPSSh/def2-TZVP)/MM values, the calculations predict rather contradictory effects. For NAAG as a substrate, calculated affinity of calcium for the active site was marginally greater for GCPIII (~ 0.5 kcal·mol^{-1}). We found the opposite pattern for BCG; the calcium substitution was ~ 10 kcal·mol^{-1} 'easier' for the GCPII-BCG complex than the GCPIII-BCG complex. Therefore, the calculations suggest that the observed differences in the catalytic efficiencies may not depend on the stability constants of calcium ions that potentially fill the partially occupied Zn2 sites. Further investigation into the observed metal ion dependence is beyond the scope of the current study.

GCPII and GCPIII expression levels can be specifically determined by enzymatic assays and correspond to mRNA levels

Based on the results obtained from the enzymological characterization of human GCPII and GCPIII, we employed the NAAG cleavage assay for specific detection of GCPII and the BCG cleavage assay for specific detection of GCPIII in a representative sample of human tissues, analogously to an earlier report [13] (Fig. 7A). Both assays were performed in the presence of calcium ions because it affords the highest difference in GCPII and GCPIII catalytic efficiencies for the substrates employed (for quantitative information, see Materials and methods). Simultaneously, we quantified the amount of mRNA coding for GCPII and GCPIII in a set of human tissues to confirm the functionality of the proposed enzymatic detection assays.

The amounts of GCPII and GCPIII transcripts were analysed in commercially available panels of human tissue cDNA libraries (Human MTC Panel I and II) by quantitative PCR (qPCR). Each transcript was amplified by a specific assay set consisting of a primer pair for amplification and a fluorescent probe for visualization. The cDNA amplification products were resolved by agarose gel electrophoresis. Besides the occasional weak formation of primer dimers in the GCPII assay set and the occasional weak formation of higher molecular weight products in the GCPIII assay, only the product of expected size was observed in all reactions. No products were formed in the negative controls without template DNA, indicating that there

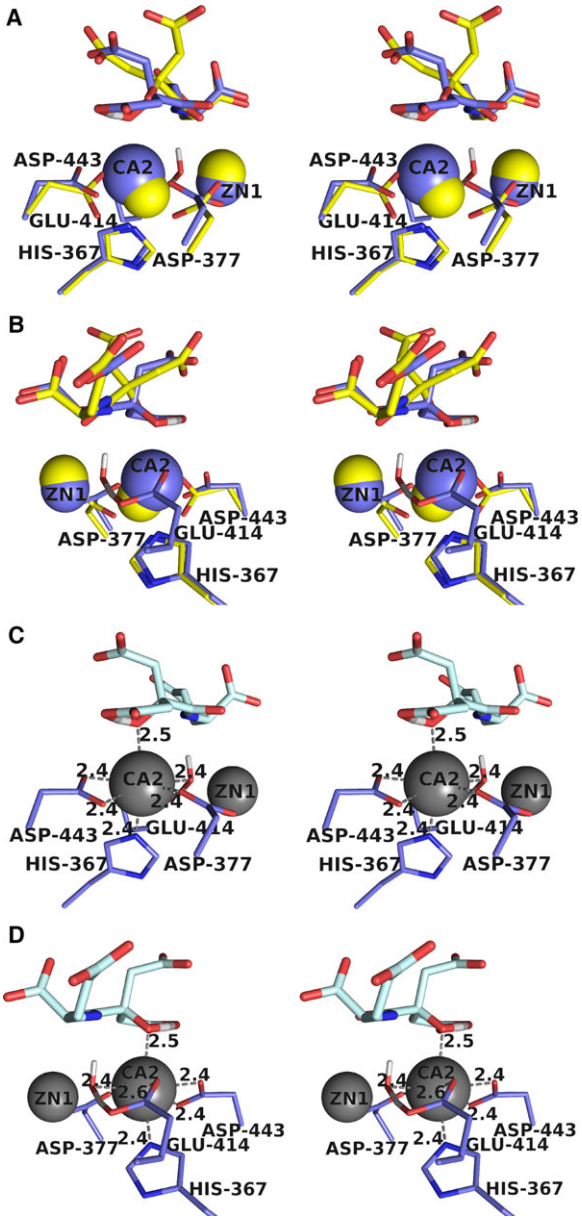

Fig. 6. QM/MM model of GCPIII in complex with BCG and with Zn2 atom replaced by calcium (II) (GCPIII-BCG-Ca2) compared to the X-ray structure of GCPII in complex with BCG (GCPII-BCG, PDB ID 5F09). Images are rendered in cross-eye stereo representation. BCG is depicted in stick representation. Please note that there is also a hydrogen atom of BCG hydroxyl group shown in light grey, which is attracted by the ionized carboxyl group of the citrate moiety, so that the hydroxyl becomes partially ionized to coordinate the Ca2 atom. Metal atoms are shown as spheres. (A) A comparison of GCPIII-BCG-Ca2 QM/MM model (blue) with GCPII-BCG (yellow). (B) The same as in (A), but rotated along *y* axis by 180°. (C) Detailed view of the coordination matrix of Ca2 in the GCPIII-BCG-Ca2 QM/MM model. BCG is coloured pale cyan, protein blue, and Zn1-Ca2 cluster grey. Coordination distances are shown in Å. (D) The same as in (C), but rotated along *y* axis by 180°.

were no false positives or negatives due to amplification of other nontargeted sequences (data not shown).

We also tested the selectivity of each assay set by amplification of plasmids with subcloned sequences of full-length GCPII or GCPIII and of isolated genomic DNA. Both assay sets amplified only the target of interest, and not the homologous transcript, and they did not tend to detect the genomic sequence. We tested selectivity against the genomic sequence because cDNA libraries are often contaminated with the genome. To this point, we also quantified the amount of the genome in the cDNA libraries by another assay set, which showed us that the contamination was very low to undetectable.

Amplification of a dilution series of plasmids with subcloned sequences of either GCPII or GCPIII showed linear dependency of determined C_q values on the logarithm of template concentration over the complete range of concentrations used. It also revealed a PCR efficiency of over 80% for both assay sets.

The absolute amounts of both transcripts detected in tissue cDNA libraries are shown in Fig. 7B. Because the cDNA libraries were normalized to several different housekeeping genes (G3PDH, alpha-tubulin, phospholipase A2, beta-actin) and are mostly pooled from multiple individuals, the results between tissues should be comparable and should represent tissue distribution of both transcripts.

As shown in Fig. 7, the protein levels of GCPII and GCPIII (Fig. 7A) determined by enzymatic assays correlate with the mRNA levels determined by qPCR (Fig. 7B). These data indicate that the enzymatic assays can be used for specific discrimination of GCPII and GCPIII expression levels in various human tissues. We detected a greater than one order of magnitude higher amount of GCPIII compared to GCPII in the testes. On the other hand, GCPIII expression in the brain, kidney and small intestine is one to two orders of magnitude lower than that of GCPII.

Discussion

In this study, we demonstrated that human GCPIII shares a similar metal-dependent enzymological profile as previously described for its mouse orthologue [13]. We observed facilitation of BCG-hydrolysing activity by Ca^{2+} ions and NAAG-hydrolysing activity by Zn^{2+} ions. Additionally, we discovered that GCPIII also processes polyglutamylated folates ($FolGlu_n$) and that this activity is facilitated by Zn^{2+} ions in a similar manner as NAAG hydrolysis.

The concentration of calcium cations used for the enzymological studies, 2.5 mM, was chosen to

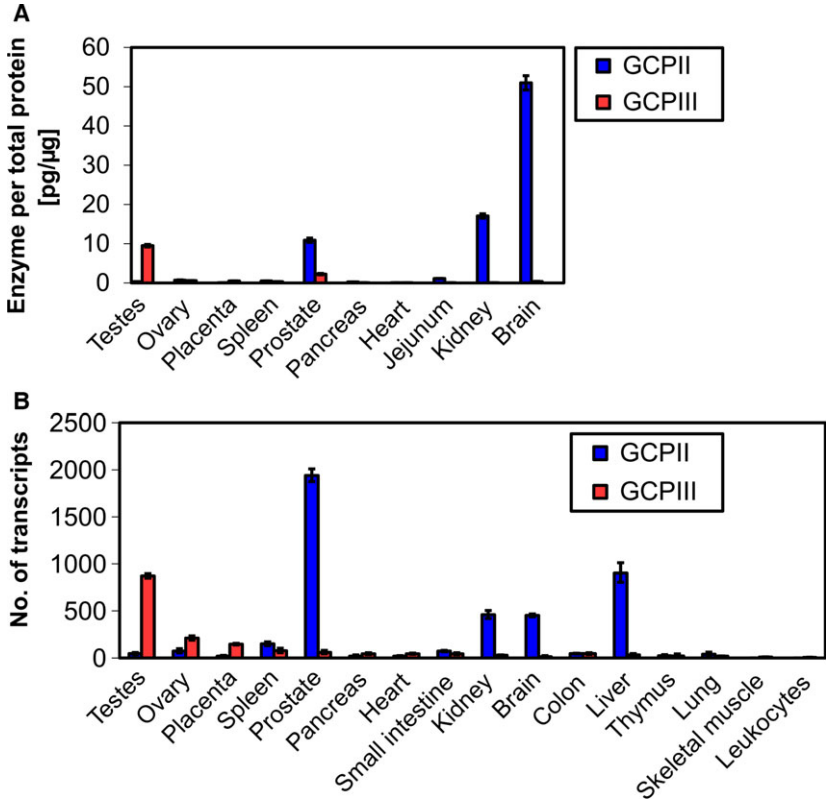

Fig. 7. GCPII/III protein and mRNA levels in human tissues. Error bars represent SD [$n = 2$ for (A), $n = 3$ for (B)]. For an easy comparison of protein and mRNA levels, tissues in (A) and (B) are juxtaposed. (A) Concentration of GCPII/III proteins in selected human tissues. The reaction buffer was 20 mM Tris, 0.15 M NaCl, 2.5 mM $CaCl_2$, 0.1% (v/v) Tween 20, pH 7.4. (B) Quantitative PCR (qPCR) determination of mRNA coding for GCPII and GCPIII. The 'No. of transcripts' shows the amount of transcripts determined in 1.0 µL of 10-fold diluted tissue cDNA library (for more experimental details see Materials and methods).

approximate the common concentrations of these cations in human plasma (despite its free, so-called ionic, concentration is usually two times lower [30]). Although free zinc concentration is very low in blood plasma [31], 0.10 mM concentration was used in our study, mainly because we wanted to characterize the saturation kinetics and because GCPIII is half-saturated by zinc at a relatively low concentration (approximately 6 µM, unpublished observation). Furthermore, zinc in the CNS serves as an orthograde, transcellular messenger [32], and it is also secreted by pancreas at the amount 1–2 mg·day^{-1} [33] (see also below). Because both metals substantially facilitated the corresponding enzymatic activities of GCPIII, GCPIII has the potential to act as either a BCG- or NAAG/FolGlu$_n$-hydrolysing enzyme. Its activity could likely be fine-tuned by the Ca^{2+} and Zn^{2+} concentrations in a particular tissue. Therefore, we suggest that GCPIII may have different enzymatic functions within the human body based on its tissue localization, the accessibility of its substrates and the concentration of divalent cations in that particular tissue. For a proper estimation of the function of GCPIII, its expression profile will need to be correlated with the distribution of its endogenous substrates, in particular BCG.

We attempted to address the structural basis for the differences in substrate specificities between these two homologues. Inspection of the GCPII and GCPIII 3D structures revealed that, although their active sites are structurally almost identical, there are two notable differences: substitution of Asn519 in GCPII with Ser509 in GCPIII and substitution of Trp541 in GCPII with Lys531 in GCPIII. The Asn to Ser substitution enables two conformations of the Zn2-coordinating amino acid Asp443 and is thus likely responsible for the lower occupancy of the Zn2 ion within the GCPIII active site [21], while the Trp to Lys substitution likely disrupts the ABS [7,20]. Disruption of the ABS in GCPIII can be exploited for development of inhibitors that are highly specific towards GCPII [34]. We corroborated these results by showing that endogenous substrates such as FolGlu$_n$, which utilize the ABS in GCPII [7], have substantially lower affinity (higher K_M value) towards GCPIII compared to GCPII. These findings suggest that even though GCPIII is also expressed at low levels in small intestine, the processing of polyglutamylated folates will likely be performed primarily by GCPII. GCPII inhibitors are currently heavily investigated as potential theranostic agents against prostate cancer [10] and various neurological disorders. Therefore, it is advisable to design compounds that would not hinder

the BCG-hydrolysing activity of its homologue GCPIII, although its physiological relevance is not quite clear yet.

Furthermore, we attempted to elucidate the mechanism of calcium-dependent BCG cleavage by determining structures of GCPII and GCPIII in complex with BCG. Unfortunately, due to experimental difficulties, we were able to prepare only protein crystals of GCPII in complex with BGC. Therefore, we built a QM/MM model of the GCPIII-BCG complex. As a control for our QM/MM approach, we also built a QM/MM structural model of GCPII in complex with NAAG and BCG (which are available as X-ray structures, PDB IDs 3BXM [22] and 5F09, respectively). The QM/MM models of GCPII in complex with NAAG or BCG and X-ray structures of inactive GCPII (Glu424Ala) in complex with these compounds are almost identical, with root-mean-square deviation values of 0.069 and 0.189 Å, respectively (except for the citrate moiety, which adopts a different conformation – the same conformation as in the GCPIII-BCG model, data not shown).

Our structural data show an overall similar binding of BCG into the GCPII and GCPIII active sites, which was expected because the major difference in the catalytic efficiencies of these two enzymes comes from substrate turnover number (k_{cat}) rather than substrate binding (K_M) (see Fig. 2B,C). Considering our observation that GCPII is not activated by divalent cations, we investigated the hypothesis that the mechanism behind the activation of GCPIII-BCG-hydrolysing activity might presumably involve replacement of the loosely coordinated Zn2 ion from GCPIII's active site with a different ion, such as Ca^{2+}. However, the QM/MM calculations did not provide a clear indication that the replacement of the Zn2 ion with Ca^{2+} would be thermodynamically more favourable for BCG as a substrate rather than NAAG and rather exclude this hypothesis. However, it should be kept in mind that QM/MM calculations do not provide any information about whether Ca^{2+} is present or absent in the partially occupied GCPIII active site. In addition, our computed values do not provide any indication whether BCG – presumably a better chelator than NAAG – assists in the Ca^{2+} uptake into the active site. This issue might be, in principle, assessed experimentally (X-ray crystallography or X-ray absorption techniques) and complemented by QM/MM/MD calculations of the activation energies of individual complexes (to analyse the kinetic origin of the observed metal ion dependency) which is well beyond the scope of the presented work.

Finally, we utilized enzymological data for specific detection of GCPII and GCPIII protein levels in several human tissues. Because there are no commercially available specific antibodies against human GCPIII, this approach represents a method for detection and discrimination between these two enzymes in human tissues. The fact that we detected lower levels of GCPIII than GCPII in brain and small intestine, the tissues where cleavage of NAAG and polyglutamylated folates, respectively, takes place, supports the assumption that BCG is the main physiological substrate of GCPIII in humans. The high level of GCPIII expression in human testes, and the high BCG-hydrolysing activity also detected in rat testes [16], further strengthens this hypothesis. We believe that a reliable determination of the GCPIII expression profile on a protein level, combined with data on BCG levels in human tissues, will help to dissect and elucidate the primary physiological function of GCPIII in the human body.

Regarding mRNA of GCPII in human tissues, there is one discrepancy to be addressed. Cunha *et al.* [35] also determined the amount of GCPII (PSMA in the medical literature) in Clontech tissue cDNA libraries. Their primers, like ours, were designed to detect only the PSMA splice variant and not the intracellular variant of PSMA. The relative PSMA expression levels in various tissues that they determined [35] are in good agreement with our results, except for PSMA expression in prostate. We determined the ratio of expression of PSMA in the prostate and liver (the tissue with second highest PSMA expression) to be approximately 2, compared to 12 in the previous report. Although the tissue libraries were normalized to four different reference genes by the vendor, Cunha *et al.* renormalized their results to only one of these genes, beta-actin. Unfortunately, they do not describe the details of the beta-actin assay or the amounts of beta-actin determined. Therefore, it is not clear whether the higher specificity of PSMA expression in their study was caused by lower levels of beta-actin in prostate, or whether the different results can be attributed to different tissue library lots.

In summary, we present a thorough enzymatic and structural characterization of the behaviour of human GCPII and GCPIII towards their physiological substrates. We also identified metal-dependent enzymatic activity of human GCPIII, which we did not observe for human GCPII. Finally, we confirmed BCG to be a specific substrate of human GCPIII. Utilizing these findings, we mapped the expression patterns of GCPII and GCPIII in a panel of human tissues. Compared to GCPII expression, we detected higher levels of

GCPIII in testes and lower levels in brain, kidney and prostate. Additionally, this study is also the first to show mRNA levels of GCPIII in the human tissues.

Materials and methods

Crystallization and data collection

Inactive GCPII with the engineered mutation Glu424Ala [22] and AviTag™ affinity tag (Avidity, Aurora, CO, USA) [19] was crystallized using the hanging drop vapour diffusion method as described earlier [36] with the following modifications: (a) 1.0 μL precipitant was added to a 1.0 μL drop of protein (concentrated to 3.6 mg·mL^{-1}) in 20 mM bistrispropane, 20 mM NaCl, pH 7.4, and sealed over a 0.50 mL reservoir of the same precipitant; (b) 0.1 μL of 2.1 mM BCG in MilliQ water (Merck Millipore, Billerica, MA, USA) was added to the crystallization drop after 11 weeks and again after 13 weeks (resulting in a calculated ratio of protein : substrate equal to 19 μM : 0.21 mM); (c) the crystal was frozen in liquid nitrogen after 15 weeks; and (d) precipitant was made up of 33% (v/v) pentaerythritol propoxylate PO/OH 5/4 (Hampton Research, Aliso Viejo, CA, USA), 1.5% (w/v) PEG 3350 (Merck KGaA, Darmstadt, Germany) and 0.10 M Tris/HCl (Merck KGaA), pH 8.0, in distilled water. In the drop, one single crystal appeared after several weeks. Crystallization approach of adding BCG right at the setup was unsuccessful. Diffraction data were collected at 100 K at the beamline BL1412 operated by the Joint Berlin MX-Laboratory at the BESSY II electron storage ring (Berlin-Adlershof, Germany) [37], using a Pilatus 6M detector (Dectris, Baden, Switzerland). Scaling and merging was done with the programs XDS [38] and its graphical user interface XDSAPP [39].

Structure determination was performed by molecular replacement using the program MOLREP from the CCP4 software package [27,40,41]. The previously solved structure of recombinant human GCPII (PDB ID 4NGP [11]) without inhibitor and water molecules was used as the starting model. Refinement calculations were performed with the program REFMAC 5.7 [42,43], and the refinement protocol was interspersed with manual corrections to the model using WINCOOT 0.7 [44]. The final models, together with experimental amplitudes, were deposited into the RCSB Protein Data Bank under the accession number 5F09. A summary of structural parameters is displayed in Table 1. Images were created with the programs PYMOL [24] and FFT and MAPMASK [45].

QM/MM calculations

All QM/MM calculations were carried out with the COMQUM program [46], which combines the quantum mechanical approach, applied to the region most relevant for the studied process, and the classical mechanical approach for the rest of the protein. In the current version, the program employs TURBOMOLE 6.6 suite [47] for the QM part and AMBER 8.0 with the *ff14SB* force field for the MM part [48]. ComQum utilizes the standard hydrogen-link approach, and the technical details of the QM/MM computational protocol have been described elsewhere [22].

All quantum chemical calculations were performed at the density functional theory (DFT) level. Geometry optimizations were carried out at the Perdew–Burke–Ernzerhof (PBE) level [49]. The DFT/PBE calculations were expedited by expanding the Coulomb integrals in an auxiliary basis set: the resolution-of-identity (RI-J) approximation. The def-SV(P) basis set was employed for all atoms. The single-point energies were then calculated using the TPSSH method [50] as implemented in TURBOMOLE 6.6. For these calculations, the def2-TZVPD basis set was employed for all atoms.

The protein (GCPII) setup

Structural models used in QM/MM calculations were based on the 1.71 Å X-ray crystallographic structure of the inactive Glu424Ala mutant of GCPII in complex with NAAG (PDB ID 3BXM [22]) and the 1.37 Å structure of the GCPIII with L-glutamate (3FF3 [21]). BCG was positioned in the active site using the GCPII (Glu424Ala)/NAAG and GCPIII/L-Glu structures as templates. The protein was equilibrated using the standard approach [22]: (a) minimizing the positions of all hydrogen atoms in the initial structure, (b) adding a solvation sphere with a radius of 50 Å (~ 12 700 and 11 500 water molecules in total for GCPII and III, respectively) and (c) running a 1 ns simulated annealing molecular dynamics followed by the final minimization of the whole system (with all nonhydrogens atoms kept at their crystallographic positions throughout). Both GCPII and GCPIII structures were neutralized by addition of ions (two Na^+ for GCPII and four Cl^- for GCPIII). We assumed the standard protonation states at pH 7 for all amino acids. For the histidine residues, the protonation status was assigned based on a detailed study of the hydrogen bond network around the residue and the solvent accessibility. In the GCPII structure, histidines 82, 347, 377, 553 and 573 were assumed to be protonated on the N^δ atom; histidines 56, 112, 124, 295, 396, 475, 689 and 697 on the N^ε atom; and histidines 345 and 618 on both nitrogens. In the GCPIII structure, histidines 124, 367, 543, 637 and 721 were assumed to be protonated on the N^δ atom; histidines 102, 285, 335, 608, 615, 679 and 687 on the N^ε atom; and histidine 72 on both nitrogens.

The quantum system consisted of ~ 280 active site atoms and is deposited in Data S1. The so-called system 2 (part of the system that is relaxed in the QM/MM calculations by MM method) comprised 48 amino acids in the vicinity

of the quantum system, and it has been selected on a per-residue based cut-off distance of 2.5 Å from the quantum system. The rest of the protein (system 3) was kept frozen in all QM/MM simulations.

Synthesis of β-citryl-L-glutamic acid (BCG)

General information

All chemicals were purchased from Sigma-Aldrich, unless stated otherwise. β-citrylglutamate (BCG) was purified using preparative scale HPLC Waters Delta 600 (Waters Corporation, Milford, MA, USA) (flow rate 7 mL·min^{-1}), with column Waters SunFire C18 OBD Prep Column, 5 μm, 19 × 150 mm (Waters Corporation). The purity of BCG was tested on the analytical Jasco PU-1580 HPLC instrument (Jasco, Easton, MD, USA) (flow rate 1 mL·min^{-1}, R_t is shown below) employing the Waters C18 Analytical Column, 5 μm, 250 × 5 mm (Waters Corporation). The final product was of at least 99% purity. Structure was further confirmed by high-resolution mass spectrometry (HRMS) at LTQ Orbitrap XL (Thermo Scientific, Waltham, MA, USA) and by NMR at Bruker Avance I™ 400 MHz (Bruker, Billerica, MA, USA).

Synthesis of β-citrylglutamate

Overall scheme for the six-step synthesis of BCG is shown below (Scheme 1). Detailed description of each step and its resulting intermediate or final compound (designated **1** to **5** or **6**, respectively) is given in the following text in the order of the synthesis (Scheme 1).

1. 2-tert-butyl 1,3-dimethyl 2-hydroxypropane-1,2,3-tricarboxylate

About 5.3 g of dimethyl citrate (24 mmol, prepared as described in [51]) was suspended in 15 mL of isobutylene and 0.5 mL of sulfuric acid was added while cooled to −78 °C. The reaction mixture cleared over time. After 18 h of stirring at room temperature, the reaction mixture was cooled down to −78 °C and poured to ice bath saturated with bicarbonate. The water phase was then washed three times by ethylacetate (EtOAc) (50 mL) and the organic

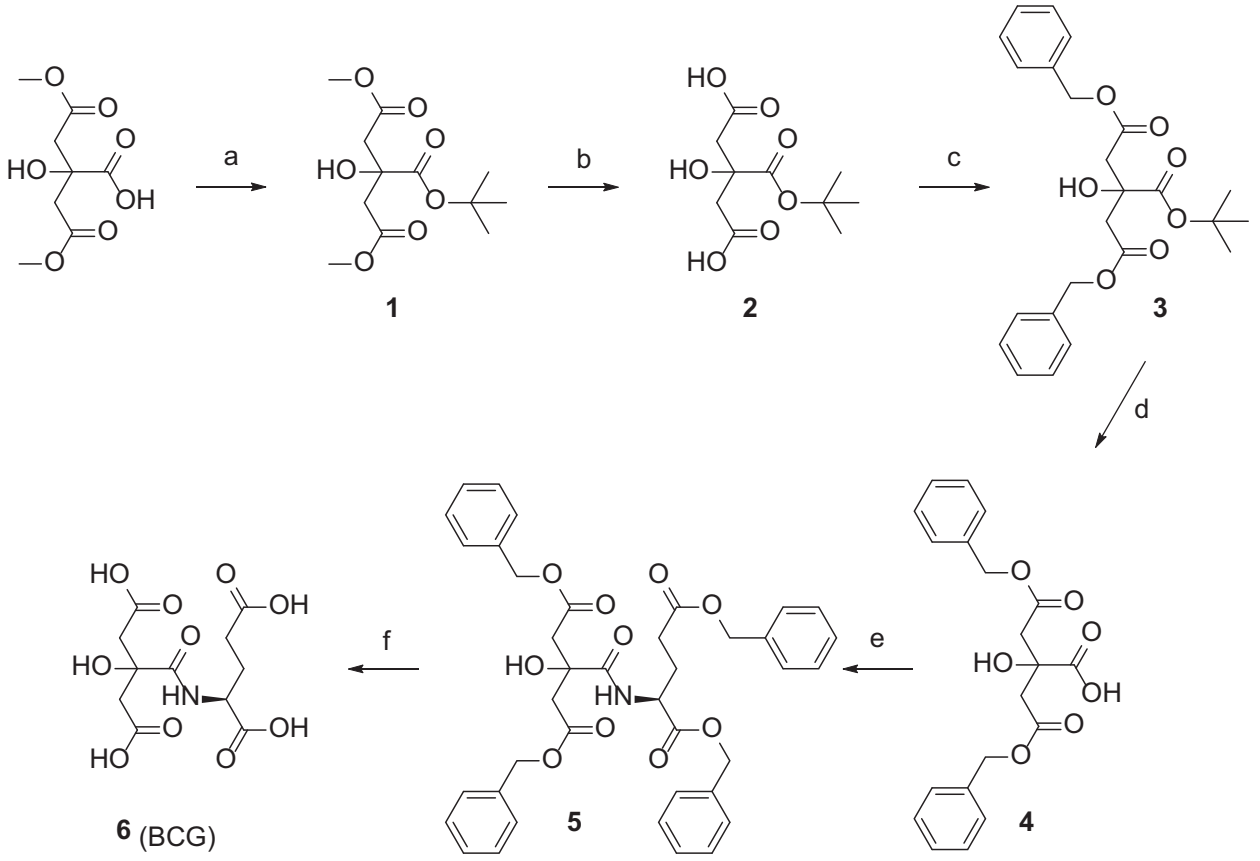

Scheme 1. The scheme for synthesis of β-citryl-L-glutamic acid (BCG). The synthesis proceeded via five intermediate compounds, designated **1**–**5**, whereby BCG is compound **6**. (a) Isobutylene, H_2SO_4; (b) NaOH, MeOH/H_2O; (c) DBU, benzyl bromide, ACN; (d) TFA; (e) NH_2Glu(OBzl)OBzl, *O*-(Benzotriazol-1-yl)-*N*,*N*,*N*′,*N*′-tetramethyluronium tetrafluoroborate, DIEA, dimethylformamide; (f) H_2, Pd(C), MeOH.

phases were combined, dried and evaporated yielding 5.3 g of pure product (yield = 80%).

2. 3-(tert-butoxycarbonyl)-3-hydroxypentanedioic acid

About 5.2 g of compound **1** (18.7 mmol) was dissolved in 20 mL of methanol and was cooled down to 0 °C. About 20 mL of 2 M NaOH was then added in portions during 5 min. The reaction was left to proceed for 6 h. The reaction mixture was then diluted by 200 mL of EtOAc and was extracted two times by 10% $KHSO_4$ (2 × 100 mL). The organic phase was then dried and evaporated to yield 3.5 g of product (yield = 75%).

3. 1,3-dibenzyl 2-tert-butyl 2-hydroxypropane-1,2,3-tricarboxylate

About 1 g of compound **2** (4.03 mmol, 1.0 eq) was suspended in 20 mL of acetonitrile (ACN) along with 1.2 mL of 1,8-Diazabicycloundec-7-ene (DBU) (8.86 mmol, 2.0 eq). About 1.05 mL of benzyl bromide was added in one portion and the reaction mixture was refluxed for 2 h. The TLC analysis (EtOAc) showed no starting material and the whole mixture was evaporated. The crude product was dissolved in 100 mL of EtOAc and was washed two times with 10% $KHSO_4$, two times with saturated $NaHCO_3$ and once with brine, and the organic phase was dried and evaporated to obtain the titled compound as white solid (1.2 g, yield = 70%). The product was used in next step without further purification (purity approximately 90%).

4. 1,3-dibenzyl 2-hydroxypropane-1,2,3-tricarboxylate

About 1.1 g of compound **3** (2.57 mmol) was dissolved in 3 mL of trifluoroacetic acid (TFA). The reaction mixture was stirred and sonicated alternately for 25 min and then the TFA was removed by flow of nitrogen. The residue was then dissolved in EtOAc and was washed three times with water to get rid of the residual TFA. The organic phase was then dried and evaporated. About 940 mg of compound **4** was obtained (yield = 95%) and it was used in the synthesis without further purification.

5. 2-{(1S)-[1,3-bis(benzylcarboxy)prop-1-yl]-carbamoyl}-1,3-bis(benzylcarboxy)-2-carboxy-2-hydroxy-propan-2-amide

About 500 mg of compound **4** (1.35 mmol, 1.1 eq) was dissolved in 5 mL of dimethylformamide along with 564 mg of 2-(1H-benzotriazol-1-yl)-1,1,3,3-tetramethyluronium hexauorophosphate (1.49 mmol, 1.1 eq) and 840 μL of *N*,*N*-Diisopropylethylamine (DIEA) (4.65 mmol, 3.5 eq). The mixture was left stirring for 15 min and then 486 mg of H_2N-Glu(OBn)-COOBn*Tos (1.49 mmol, 1.0 eq) was added in one portion. After 2.5 h, all volatiles were evaporated and the residue was dissolved in 50 mL of EtOAc. The organic phase was washed two times with 10% $KHSO_4$, two times with saturated $NaHCO_3$ and once with brine. About 600 mg of compound **5** (yield = 60%) was obtained as an oily product after evaporation and column chromatography on silica (EtOAc, TLC R_f = 0.25).

6. 3-{[(1S)-1,3-dicarboxypropyl]carbamoyl}-3-hydroxy-pentanedioic acid (ß-citrylglutamate, BCG)

About 50 mg of compound **5** was dissolved in 2 mL of methanol (MeOH) and catalytical amount of palladium on activated charcoal [Pd(C)] was added. The reaction mixture was first purged with flow of nitrogen, then with flow of hydrogen. The benzyl groups were then removed during 3 h using slightly elevated pressure of hydrogen (1.05 Atm). TLC analysis showed that all the reactants disappeared and the reaction mixture was filtered and evaporated. The product was purified using preparative scale HPLC (isocratic 2.5% ACN, R_t = 6 min). About 10 mg was isolated upon dry freezing (isolated yield = 42%). ^{1}H NMR (401 MHz, DMSO) δ 12.31 (bs, 4H), 7.74 (d, J = 8.0 Hz, 1H), 5.73 (bs, 1H), 4.25 (td, J = 8.3, 4.8 Hz, 1H), 2.77 (d, J = 15.6 Hz, 1H), 2.68 (d, J = 15.7 Hz, 1H), 2.66 (d, J = 15.2 Hz, 1H), 2.58 (d, J = 15.2 Hz, 1H), 2.37–2.21 (m, 2H), 2.07–1.98 (m, 1H), 1.89–1.78 (m, 1H). ^{13}C NMR (101 MHz, DMSO) δ 174.01, 173.40, 172.94, 171.41, 171.26, 73.47, 51.12, 42.90, 42.45, 29.66, 26.78. Analytical HPLC R_t = 4.0 min. HRMS (ESI-) m/z for $C_{19}H_{22}O_7N_2$ $[M-H]^-$ calculated 389.13433, found 389.13424.

Expression and purification of recombinant human GCPII, GCPIII and GCPII inactive variant

The expression and purification protocols for all used human recombinant proteins in this study, Avi-tagged extracellular portion of GCPII [19], GCPIII [12], the inactive variant of GCPII [7] and tag-free extracellular portion of GCPII [52], have been described earlier.

GCPII and GCPIII activity assay

Because GCPIII activity is metal-dependent, MilliQ (Merck Millipore) was used to prepare all solutions. Reactions with BCG, NAAG (Merck KGaA) and folyl-*n*-γ-L-glutamic acids ($FolGlu_{1-6}$) (Schircks Laboratories, Jona, Switzerland) were performed in 25 mM Tris/HCl, pH 7.5, (Merck KGaA) or 25 mM bistrispropane HCl, pH 7.5, (Merck KGaA) in a total volume of 215 μL in a 96-well plate immersed in a water bath (Grant Instruments, Shepreth, UK) at 37.0 °C [or in a lower throughput setting in 1.5 mL eppendorf tubes using a thermo-block Bioer MB120 (MB-102; Bioer, Hangzhou, China)]. Concentrations of substrate stock solutions were determined by amino acid analysis [53]. All components were pipetted on ice, and reactions

were started by adding substrate following a 5- to 13-min preincubation at 37.0 °C. After 20 min, the reactions were terminated by inhibiting the enzyme and by changing the pH to 5.8 by addition of 10.0 μL stopping solution composed of 0.37 M phosphoric acid (Penta, Prague, Czech Republic) and 22 μM 2-(phosphonomethyl)-pentanedioic acid in MilliQ water (Merck Millipore) (when 25 mM bis-trispropane buffer, pH 7.5, was used) or 3.48 μL of 0.41 M phosphoric acid (Penta), 72 μM 2-(phosphonomethyl)-pentanedioic acid and 7.2 μM 2-mercaptoethanol (Merck KGaA) in MilliQ water (Merck Millipore) (when 25 mM Tris/HCl buffer, pH 7.5, was used). Reaction conditions were designed to yield 10–30% substrate turnover. The method for quantifying $FolGlu_{1-6}$ substrates and $FolGlu_{0-5}$ products was the same as described elsewhere [7], while hydrolysis of NAAG and BCG was assessed with a novel assay (see below for details). Using GraFit, we fitted a saturation curve to 6–11 data points for every substrate (whereby each point represented a single or average of a duplicate experiment). Because of low K_M values, the assay was sometimes restricted by the limit of quantification of the employed analytic method (indicated by an asterisk in Fig. 2 and below), meaning that the K_M value was smaller than the lowest experimental substrate concentration. In Fig. 2, the lowest substrate concentrations were, from left to right, 1.5, 0.20, 0.20, 0.20, 0.32*, 0.088*, 0.20, 0.20, 0.20, 0.10, 0.14*, 0.045, 0.031, 0.030, 0.034 μM.

Quantification of glutamate in the enzymatic assay

To quantify glutamate as a product of NAAG and BCG cleavage, a novel method was developed. It is based on a highly concentrated solution of orthophthalaldehyde (OPA), a commonly used reagent for amino acid derivatization [53]. The new derivatization formulation was a 0.10 M OPA, 0.30 M 3-mercaptopropionic acid, 4% acetonitrile (v/v) and 0.94 M bistrispropane, pH 9.6 solution. A 11.0 μL portion of the solution was added to 99 μL of a reaction containing the cleavage product glutamate. This improvement made it possible to surpass the need to concentrate the sample by lyophilization and redissolving it [7]. Sample derivatization and analysis was performed on an Agilent 1200 or 1260 instrument (Agilent Technologies, Santa Clara, CA, USA) similarly as described previously [7], except that the analysis method was slightly modified. The new method consisted of 13.80 min at 0.7% B, 0.05 min transition to 80.0% B, 1.00 min at 80.0% B, 0.05 min transition back to 0.70% B, 0.60 min at 0.7% B, injection of 20.0 μL of 16-fold diluted 85% phosphoric acid (w/w; Penta), pH 2.5, (NaOH; Penta) to dissolve precipitate of metal hydroxides, and 10.50 min at 0.7% B. The automatic derivatization procedure and injection performed by the instrument just prior to analysis took approximately 7 min.

Atomic absorption spectroscopy to determine Zn occupancy in the GCPIII active site

Following purification, approximately 10 μM GCPII and GCPIII was dialysed against 10 mM MOPS (Duchefa, Biochemie, Haarlem, the Netherlands; pH adjusted by KOH), pH 7.4, using Slide-A-Lyzer™ MINI Dialysis Devices (Thermo Scientific). The buffer was prepared from MilliQ water (Merck Millipore) and subjected to Chelex 100 (Bio-Rad, Hercules, CA, USA) before use. Dialysis devices and glass vials used for protein preparation were washed twice with EDTA solution and thoroughly with MilliQ (Merck Millipore) water. Samples were analysed on an Analyst 800 spectrometer (Perkin-Elmer, Waltham, MA, USA) with electrothermal atomization using an EDL Zn lamp. Temperatures of pyrolysis and atomization were 700 °C and 1500 °C, respectively. Palladium was employed as a modifier. The limit of detection for zinc was 0.1 $ng \cdot mL^{-1}$. For the analysis itself, samples were diluted 200-fold. The analysed volume was 10 mL. Measurements were performed at least in triplicate. The protein concentration was quantified by amino acid analysis [53].

Quantification of GCPII/III at the protein and mRNA levels

Enzymatic assay

The total protein concentrations of tissue lysates were estimated by a modified Bradford method (Protein Assay; Bio-Rad), using BSA (Thermo Scientific) as a standard and 97 mM HEPES (Merck KGaA) and 0.15 M NaCl (Penta) pH 7.5 (NaOH; Penta) as a buffer. For the activity assay, tissue lysates were diluted 5.3- to 7300-fold overall. Buffer used for the specific detection of both GCPII and GCPIII was prepared from MilliQ water (Merck Millipore), composed of 20 mM Tris (Merck KGaA), 0.15 M NaCl (Penta), 2.5 mM $CaCl_2$ (Merck KGaA) and 0.1% (v/v) Tween 20 (USB, Cleveland, OH, USA), pH 7.4 (HCl, Penta) and filtered through a 0.22 μm filter (Merck Millipore). As a substrate, [^{3}H]NAAG and [^{3}H]BCG were used at 5 nM final concentration (mixed with cold substrates in a 19 : 1 molar ratio to yield a total substrate concentration of 100 nM) in a previously described radiometric assay [5], in which the column volume was 1.0 or 0.5 mL and elution was performed with 2.4 or 1.2 mL of 1 M HCOOH (Penta), respectively. The usual time of incubation was 17 h at 37.0 °C.

This particular buffer confers the needed differences in specificities of GCPII towards NAAG and GCPIII towards BCG: When GCPII is quantified according to NAAG hydrolysis, GCPIII must be approximately 60-fold more concentrated to yield a comparable turnover. On the other hand, when GCPIII is quantified according to BCG hydrolysis, GCPII does not cleave BCG at all even if its concentration is 180-fold higher (data not shown).

Quantitative PCR

Amounts of GCPII transcript (encoded by the gene FOLH1) were quantified by an assay set of forward and reverse primers (sequences 5′-CGG CTT CCT CTT CGG GTG-3′ and 5′-GAT GTT CTC AGC TTT CAA TTC ATC C-3′) and a fluorescent hydrolysis probe (sequence 5′-ATC CTC CAA TGA AGC TAC TAA CAT TAC TCC AA-3′). This set was designed to amplify nucleotides 366–471 in the GCPII transcript (NM_004476) to yield an amplified product of 106 bps, which covers regions of exons 1 and 2 and corresponds to amino acids 35–70 in the longest open reading frame (ORF). The forward primer is complementary to the exon 1–exon 2 junction, and it was designed to enable selective amplification of the wild-type GCPII protein-coding splice variant (usually termed PSMA). This assay set was also designed to amplify neither genomic sequences nor the prostate specific membrane antigen like protein transcript, which is encoded by the pseudogene FOLH1B.

Amounts of GCPIII transcript were quantified by an assay set of forward and reverse primers (sequences 5′-TTT GGA CTT CTG GGT TCC AC-3′ and 5′-TGC TTC TCT CCT GGA GTA TTT TG-3′) and a fluorescent hydrolysis probe, Universal probe #30 (Roche, 04687639001, Basel, Switzerland). This set was designed to amplify nucleotides 1291–1354 in the GCPIII transcript (NM_005467) which covers regions in exons 11 and 12 and corresponds to amino acids 416–437 in the longest ORF. The expected size of the amplified product was 64 bases; the size of a possibly amplified genomic DNA sequence was 5308 bases.

As a standard for absolute quantification, serial 10-fold dilutions covering concentrations from 10^7 to 10^2 copies per reaction of pcDNA4 plasmid with subcloned protein-coding sequence of either GCPII (longest ORF from NM_004476 coding amino acids 1–750, i.e. full-length GCPII) or GCPIII (longest ORF from NM_005467 coding amino acids 1–740, i.e. full-length GCPIII) were amplified with both assay sets. The initial concentration of plasmid DNA (purified by QIAprep Spin Miniprep Kit; Qiagen, Venlo, Netherlands) prior to dilution was determined spectrophotometrically by absorption at 260 nm (Nanodrop ND-1000; Thermo Scientific). To enable precise comparison between the determined amounts of both transcripts, obtained calibration curves were further normalized against each other by quantification of common regions in both plasmids. The ampicillin resistance gene region was quantified with a set of primers of sequences 5′-GCA GAA GTG GTC CTG CAA CT-3′ and 5′-AGC TTC CCG GCA ACA ATT A-3′ and Universal probe #58 (Roche). In this way, two calibration curves were obtained for each plasmid, one for the amplification of target transcript and one for the common sequence. Finally, the slope and intercept values of both curves were transformed for each plasmid so that the transformed slope and intercept values of the curves for the common sequence were equal and corresponded to the average value between the two plasmids.

To assess the selectivity of qPCR amplification, both pcDNA4 plasmids with subcloned protein-coding sequences of either GCPII or GCPIII (10^6 copies per reaction) were amplified in the same qPCR setup by both assay sets, and possible products were inspected by agarose gel electrophoresis. For the same reason, amplification of isolated human genomic DNA was tested in the same way. The amount of genomic DNA was quantified by a set of primers of sequences 5′-GAG AAC CGT TTG AAT GAA ACT GAG-3′ and 5′-TTG GAT GAA CAG GAA TAC TTG GAA GA-3′ and a fluorescent hydrolysis probe of sequence 5′-ACA GCC TCT GCA ATT CCA CGC CTA T-3′, which detects the intron–exon junction of the FOLH1 gene (gene coding for GCPII).

The amount of both GCPII and GCPIII transcripts was then measured in 1.0 μL of 10-fold diluted tissue cDNA libraries obtained from Clontech (Human MTC Panel I and II; Takara Bio, Kyoto, Japan).

All qPCR reactions were carried out in triplicate in FrameStar 480/96 multiwell plates (4titude, Dorking, UK) sealed with adhesive foil (Roche) using a LightCycler 480 II instrument (Roche) in a total volume of 10 μL. Each reaction consisted of a LightCycler 480 Probe Master (Roche) diluted according to the manufacturer's instructions, forward and reverse primer (1 μM final concentration each), fluorescent probe (final concentration of Roche universal probes was 50 nM; final concentration of custom probes was 100 nM) and 1 μL of sample or template DNA (positive and nontemplate controls as well as interplate calibrators were included on each plate). Initial denaturation for 3 min at 95 °C was followed by 45 cycles of 10 s at 95 °C, 30 s at 66 °C and 30 s at 72 °C. The threshold cycle numbers (C_q) were then determined from fluorescence intensities acquired during the qPCR runs by second derivative maximum method using LIGHTCYCLER 480 software (Roche). The presence and the size of PCR products was analysed in all qPCR reactions by agarose gel electrophoresis.

Acknowledgements

We thank Prof Barbara Slusher (School of Medicine, John Hopkins University, MD, USA) for her kind gift of the 2-PMPA inhibitor; Radko Souček for amino acid analysis; Dr Sebastian Zoll for data collection, scaling and molecular replacement; Jana Starková for cultivation of S2 cells; Dr Vlasta Korunová for AAS; and Dr Pavel Šácha for recloning the inactive GCPII Glu424Ala into the vector pMT/Bip/AviTEV/rhGCPII. The financial support of the Czech Science Foundation (GA CR, projects P208-12-G016 and 14-31419S) and InterBioMed I project LO 1302 and

LO 1304 (to PP) from the Ministry of Education of the Czech Republic is gratefully acknowledged.

Author contributions

MN performed protein purification, crystallization and kinetic studies; JT and PP performed X-ray structure refinement and validation; JS synthesized BCG; KH prepared protein samples for AAS; LR and TAR worked out the QM/MM models; VN quantified GCPII/III in human tissues; JK initiated and led the project; MN, JT, LR, KH, VN and JK analysed the data and wrote the manuscript.

References

1 Hlouchova K, Navratil V, Tykvart J, Sacha P & Konvalinka J (2012) GCPII variants, paralogs and orthologs. *Curr Med Chem* **19**, 1316–1322.
2 Pangalos MN, Neefs JM, Somers M, Verhasselt P, Bekkers M, van der Helm L, Fraiponts E, Ashton D & Gordon RD (1999) Isolation and expression of novel human glutamate carboxypeptidases with N-acetylated alpha-linked acidic dipeptidase and dipeptidyl peptidase IV activity. *J Biol Chem* **274**, 8470–8483.
3 Hlouchova K, Barinka C, Klusak V, Sacha P, Mlcochova P, Majer P, Rulisek L & Konvalinka J (2007) Biochemical characterization of human glutamate carboxypeptidase III. *J Neurochem* **101**, 682–696.
4 Bzdega T, Crowe SL, Ramadan ER, Sciarretta KH, Olszewski RT, Ojeifo OA, Rafalski VA, Wroblewska B & Neale JH (2004) The cloning and characterization of a second brain enzyme with NAAG peptidase activity. *J Neurochem* **89**, 627–635.
5 Robinson MB, Blakely RD, Couto R & Coyle JT (1987) Hydrolysis of the brain dipeptide N-acetyl-L-aspartyl-L-glutamate. Identification and characterization of a novel N-acetylated alpha-linked acidic dipeptidase activity from rat brain. *J Biol Chem* **262**, 14498–14506.
6 Chandler CJ, Wang TTY & Halsted CH (1986) Pteroylpolyglutamate hydrolase from human jejunal brush-borders – purification and characterization. *J Biol Chem* **261**, 928–933.
7 Navratil M, Ptacek J, Sacha P, Starkova J, Lubkowski J, Barinka C & Konvalinka J (2014) Structural and biochemical characterization of the folyl-poly-gamma-L-glutamate hydrolyzing activity of human glutamate carboxypeptidase II. *FEBS J* **281**, 3228–3242.
8 Huber F, Montani M, Sulser T, Jaggi R, Wild P, Moch H, Gevensleben H, Schmid M, Wyder S & Kristiansen G (2015) Comprehensive validation of published immunohistochemical prognostic biomarkers of prostate cancer—what has gone wrong? A blueprint for the way forward in biomarker studies. *Br J Cancer* **112**, 140–148.
9 Queisser A, Hagedorn SA, Braun M, Vogel W, Duensing S & Perner S (2015) Comparison of different prostatic markers in lymph node and distant metastases of prostate cancer. *Mod Pathol* **28**, 138–145.
10 Foss CA, Mease RC, Cho SY, Kim HJ & Pomper MG (2012) GCPII imaging and cancer. *Curr Med Chem* **19**, 1346–1359.
11 Tykvart J, Schimer J, Barinkova J, Pachl P, Postova-Slavetinska L, Majer P, Konvalinka J & Sacha P (2014) Rational design of urea-based glutamate carboxypeptidase II (GCPII) inhibitors as versatile tools for specific drug targeting and delivery. *Bioorg Med Chem* **22**, 4099–4108.
12 Tykvart J, Navratil V, Sedlak F, Corey E, Colombatti M, Fracasso G, Koukolik F, Barinka C, Sacha P & Konvalinka J (2014) Comparative analysis of monoclonal antibodies against prostate-specific membrane antigen (PSMA). *Prostate* **74**, 1674–1690.
13 Collard F, Vertommen D, Constantinescu S, Buts L & Van Schaftingen E (2011) Molecular identification of beta-citrylglutamate hydrolase as glutamate carboxypeptidase 3. *J Biol Chem* **286**, 38220–38230.
14 Miyake M, Kakimoto Y & Sorimachi M (1978) Isolation and identification of beta-citryl-L-glutamic acid from newborn rat-brain. *Biochim Biophys Acta* **544**, 656–666.
15 Miyake M, Kume S & Kakimoto Y (1982) Correlation of the level of beta-citryl-L-glutamic acid with spermatogenesis in rat testes. *Biochim Biophys Acta* **719**, 495–500.
16 Miyake M, Innami T & Kakimoto Y (1983) A beta-citryl-L-glutamate-hydrolysing enzyme in rat testes. *Biochim Biophys Acta* **760**, 206–214.
17 Hamada-Kanazawa M, Kouda M, Odani A, Matsuyama K, Kanazawa K, Hasegawa T, Narahara M & Miyake M (2010) Beta-citryl-L-glutamate is an endogenous iron chelator that occurs naturally in the developing brain. *Biol Pharm Bull* **33**, 729–737.
18 Rovenská M, Hlouchová K, Sácha P, Mlcochová P, Horák V, Zámecník J, Barinka C & Konvalinka J (2008) Tissue expression and enzymologic characterization of human prostate specific membrane antigen and its rat and pig orthologs. *Prostate* **68**, 171–182.
19 Tykvart J, Sacha P, Barinka C, Knedlik T, Starkova J, Lubkowski J & Konvalinka J (2012) Efficient and versatile one-step affinity purification of in vivo biotinylated proteins: expression, characterization and structure analysis of recombinant human glutamate carboxypeptidase II. *Protein Expr Purif* **82**, 106–115.
20 Zhang AX, Murelli RP, Barinka C, Michel J, Cocleaza A, Jorgensen WL, Lubkowski J & Spiegel DA (2010) A remote arene-binding site on prostate specific membrane antigen revealed by antibody-recruiting small molecules. *J Am Chem Soc* **132**, 12711–12716.

21 Hlouchova K, Barinka C, Konvalinka J & Lubkowski J (2009) Structural insight into the evolutionary and pharmacologic homology of glutamate carboxypeptidases II and III. *FEBS J* **276**, 4448–4462.
22 Klusak V, Barinka C, Plechanovova A, Mlcochova P, Konvalinka J, Rulisek L & Lubkowski J (2009) Reaction mechanism of glutamate carboxypeptidase II revealed by mutagenesis, X-ray crystallography, and computational methods. *Biochemistry* **48**, 4126–4138.
23 Mesters JR, Barinka C, Li WX, Tsukamoto T, Majer P, Slusher BS, Konvalinka J & Hilgenfeld R (2006) Structure of glutamate carboxypeptidase II, a drug target in neuronal damage and prostate cancer. *EMBO J* **25**, 1375–1384.
24 DeLano WL (2004) Use of PYMOL as a communications tool for molecular science. *Abstr Pap Am Chem Soc* **228**, U313–U314.
25 Diederichs K & Karplus PA (1997) Improved R-factors for diffraction data analysis in macromolecular crystallography. *Nat Struct Biol* **4**, 269–275.
26 Vaguine AA, Richelle J & Wodak SJ (1999) SFCHECK: a unified set of procedures for evaluating the quality of macromolecular structure-factor data and their agreement with the atomic model. *Acta Crystallogr D* **55**, 191–205.
27 Dodson EJ, Winn M & Ralph A (1997) Collaborative computational project, number 4: providing programs for protein crystallography. *Methods Enzymol* **277**, 620–633.
28 Davis IW, Leaver-Fay A, Chen VB, Block JN, Kapral GJ, Wang X, Murray LW, Arendall WB, Snoeyink J, Richardson JS *et al.* (2007) MolProbity: all-atom contacts and structure validation for proteins and nucleic acids. *Nucleic Acids Res* **35**, W375–W383.
29 Chen VB, Arendall WB III, Headd JJ, Keedy DA, Immormino RM, Kapral GJ, Murray LW, Richardson JS & Richardson DC (2010) MolProbity: all-atom structure validation for macromolecular crystallography. *Acta Crystallogr D* **66**, 12–21.
30 Ryden SE, Kirkish LS & McCann DS (1976) Evaluation of serum ionic calcium measurement in a general hospital population. *Am J Clin Pathol* **66**, 634–638.
31 Magneson GR, Puvathingal JM & Ray WJ (1987) The concentrations of free Mg2 + and free Zn2 + in equine blood plasma. *J Biol Chem* **262**, 11140–11148.
32 Frederickson CJ, Suh SW, Silva D, Frederickson CJ & Thompson RB (2000) Importance of zinc in the central nervous system: the zinc-containing neuron. *J Nutr* **130**, 1471s–1483s.
33 Kelleher SL, McCormick NH, Velasquez V & Lopez V (2011) Zinc in specialized secretory tissues: roles in the pancreas, prostate, and mammary gland. *Adv Nutr* **2**, 101–111.
34 Tykvart J, Schimer J, Jančařík A, Bařinková J, Navrátil V, Starková J, Šrámková K, Konvalinka J, Majer P & Šácha P (2015) Design of highly potent urea-based, exosite-binding inhibitors selective for glutamate carboxypeptidase II. *J Med Chem* **58**, 4357–4363.
35 Cunha AC, Weigle B, Kiessling A, Bachmann M & Rieber EP (2006) Tissue-specificity of prostate specific antigens: comparative analysis of transcript levels in prostate and non-prostatic tissues. *Cancer Lett* **236**, 229–238.
36 Barinka C, Starkova J, Konvalinka J & Lubkowski J (2007) A high-resolution structure of ligand-free human glutamate carboxypeptidase II. *Acta Crystallogr F* **63**, 150–153.
37 Mueller U, Darowski N, Fuchs MR, Förster R, Hellmig M, Paithankar KS, Pühringer S, Steffien M, Zocher G & Weiss MS (2012) Facilities for macromolecular crystallography at the Helmholtz-Zentrum Berlin. *J Synchrotron Radiat* **19**, 442–449.
38 Kabsch W (2010) Xds. *Acta Crystallogr D* **66**, 125–132.
39 Krug M, Weiss MS, Heinemann U & Mueller U (2012) XDSAPP: a graphical user interface for the convenient processing of diffraction data using XDS. *J Appl Crystallogr* **45**, 568–572.
40 Vagin A & Teplyakov A (2000) An approach to multi-copy search in molecular replacement. *Acta Crystallogr D* **56**, 1622–1624.
41 Bailey S (1994) The Ccp4 suite – programs for protein crystallography. *Acta Crystallogr D* **50**, 760–763.
42 Murshudov GN, Vagin AA & Dodson EJ (1997) Refinement of macromolecular structures by the maximum-likelihood method. *Acta Crystallogr D* **53**, 240–255.
43 Murshudov GN, Skubak P, Lebedev AA, Pannu NS, Steiner RA, Nicholls RA, Winn MD, Long F & Vagin AA (2011) REFMAC5 for the refinement of macromolecular crystal structures. *Acta Crystallogr D* **67**, 355–367.
44 Emsley P, Lohkamp B, Scott WG & Cowtan K (2010) Features and development of Coot. *Acta Crystallogr D* **66**, 486–501.
45 Winn MD, Ballard CC, Cowtan KD, Dodson EJ, Emsley P, Evans PR, Keegan RM, Krissinel EB, Leslie AGW, McCoy A *et al.* (2011) Overview of the CCP4 suite and current developments. *Acta Crystallogr D* **67**, 235–242.
46 Ryde U & Olsson MHM (2001) Structure, strain, and reorganization energy of blue copper models in the protein. *Int J Quantum Chem* **81**, 335–347.
47 Ahlrichs R, Bär M, Häser M, Horn H & Kölmel C (1989) Electronic structure calculations on workstation computers: the program system turbomole. *Chem Phys Lett* **162**, 165–169.
48 Maier JA, Martinez C, Kasavajhala K, Wickstrom L, Hauser KE & Simmerling C (2015) ff14SB: improving the accuracy of protein side chain and backbone parameters from ff99SB. *J Chem Theory Comput* **11**, 3696–3713.

49 Perdew JP, Burke K & Ernzerhof M (1996) Generalized gradient approximation made simple. *Phys Rev Lett* **77**, 3865–3868.
50 Tao J, Perdew JP, Staroverov VN & Scuseria GE (2003) Climbing the density functional ladder: nonempirical meta-generalized gradient approximation designed for molecules and solids. *Phys Rev Lett* **91**, 146401.
51 Guo HY, Naser SA, Ghobrial G & Phanstiel O (2002) Synthesis and biological evaluation of new citrate-based siderophores as potential probes for the mechanism of iron uptake in mycobacteria. *J Med Chem* **45**, 2056–2063.
52 Barinka C, Rinnova M, Sacha P, Rojas C, Majer P, Slusher BS & Konvalinka J (2002) Substrate specificity, inhibition and enzymological analysis of recombinant human glutamate carboxypeptidase II. *J Neurochem* **80**, 477–487.
53 Roth M (1971) Fluorescence Reaction for Amino Acids. *Anal Chem* **43**, 880–882.

Supporting information

Additional Supporting Information may be found online in the supporting information tab for this article:
Data S1. Supplementary information.